Chapter

Spectral Characterization and Analysis of Underground Optical Fibre Cable Network Using Optical Time Domain Reflectometry

Asiya E. Asiya, Michael U. Onuu, Rufus C. Okoro and O. Enendu Uche

Abstract

Many of the optical fibre cables comprised of 1310 nm zero-dispersion single-mode (SM) optical fibres installed in underground/conduits and access networks. Currently, there have been several studies on active network systems, which are designed to increase transmission capacity and flexibility. The application of active communication devices like the wavelength division multiplexing (WDM) systems, usually using SM optical fibre for transmission in the 1310–1625 nm window wavelength, proves very effective in decreasing the installation costs and high signal attenuations. It was imperative to examine the wavelength dependency of such transmission characteristics of SM optical fibre cables previously installed and in which several optical fibres were spliced. Analysis for such network has been performed and monitored over 1550–1625 nm wavelength. Results show that the spectral characterization and analysis of a long-haul optical network system operating at the 50-GHz-spaced 80-dense wavelength division multiplexing (DWDM)-channel can be used to identify the presence of faults.

Keywords: optical fibre cable, attenuation, chromatic dispersion, polarization mode dispersion, OSNR, WDM

1. Introduction

An optical network is a communications network in which the transmission links are made up of optical fibres and whose architecture aims at exploring optical fibre advantages such as high speed, higher bandwidth, greater reliability and lower maintenance cost [1].

The deployment of optical fibre cable as a backbone for the transmission of data is becoming more and more prevalent in the field of telecommunications. Telephone and cable companies and internet service providers, in collaboration with government authorities, for example, are continuously expanding their fibre networks to reach more consumers across a wider geographic area. Even though it is unlikely that there

will be a need for gigabit speeds for desktop and home appliances (IoTs) any time soon, many applications are outgoing their 10 and 100 Mbps ethernet LANs [2].

Currently, most Chinese information capacity is transferred over the optic cable line. With the increase of optic fibre cable faults and optical fibre cable ageing, the frequency of optic fibre line faults increases, and it is difficult to detect fault's location in the traditional optical fibre management mode. It will take a long time to eliminate the failure factor that affects the regular work of the network [3]. Although nowadays ring network protection technology can guarantee smooth and continuous transmission to a certain extent, the shortcoming of traditional line maintenance still exists. Therefore, the implementation of the optic fibre cable line real-time detection and management, dynamic observations of the transmission properties of the optic fibre cable line degradation and the timely discovery may prevent hidden trouble and reduce the incidence of signal delaying. However, such management systems may only inform the maintainers when a fault happens but cannot detect the exact location of the fault.

During installation, cables or connectors may be broken, and other impacts such as bilging, stress and ageing on the cable and active devices can lead to faults in the entire transmission system. Such failures may result in economic loss and also causes great inconvenience to users' social well-being [4]. Therefore, it is essential to ensure the wellness of fibre optic cable. Repair and maintenance of cable communication have profound significance. The practical approach to faults determination focuses on measuring the faults distance of optical cables and the Euclidean distance to the earth's surface [5] between the optical transmitter and the point in the underground cable cut. However, the solution proposed in Ref. [6] introduced several cable junctions along the fibre optic cable transmission line, which ultimately increased the loss in the underground fibre optic network [7–9].

In engineering new optical systems on an older fibre link, it is frequently necessary to repair existing faults and other links between fibre optic cables. When technicians are called to the field to repair or modify fibre faults, they rely on manually produced maps to identify the proper location to dig for the cables. Because most underground optical fibre cable is buried adjacent to railroad tracks, digging becomes very expensive due to the extensive governmental procedures like giving right of way and, on the other hand, contract crews necessary to flag the railroad and traffic. A failed attempt to locate a fibre optic cable thus results in increased costs due to longer service times, the cost of restoring the improperly excavated area and the opportunity to damage other underground equipment that may be buried where the fibre optic cables were thought to be located.

In this paper, the authors examine the wavelength dependency of long-haul underground SM fibre optic cable networks and their corresponding active components with the view to characterize the spectral dependency of such communication network systems. It was possible to detect and trace faults with minimal error on the optical fibre cable network using the principle of the backscattering method of the optical time-domain reflectometer.

2. Literature review

According to work done in Refs. [5, 10], simulation and laboratory work provide relevant expected results in determining faults in the network. Various tools were used to conduct a series of laboratory, field and classroom experiments to achieve the

accuracy of vulnerability tracing. These tools use different scientific principles, tools and measurement techniques to measure distances during troubleshooting. Previous studies on these scientific principles and other techniques include flaw detection using OTDR [11], a photonic probe flaw locator, Raman fibre sensor, T-OTDR, correlation technique using traffic signal and step frequency method [12]. Reviews of articles on fault detection focus mainly on fibre optic cables, except in Ref. [13], which provide theoretical results of FOC to fault distance measurement on the earth's surface. The mean time to repair (MTTR) of fault tracing in underground optical networks is high due to the complex processes involved. The distance from faults in the underground fibre optic network must be accurately and timely determined and correctly connected to restore interrupted services and maintain the region's customer experience. This can only be achieved if an intelligent system is integrated into the tracing technique for the prediction of fault distances on earth [14–17]. In this regard, the author in Ref. [18] has proposed an artificial intelligence model to complement the functions of conventional OTDRs.

2.1 Spectral characterization of optical fibre

The spectral characteristics of an optical fibre network may be categorized as linear or non-linear. The non-linear characteristics are subjective to some factors, like bit rates, channel spacing and power levels [19]. While the linear characteristics include attenuation, chromatic dispersion (CD), polarization mode dispersion (PMD) and optical signal-to-noise ratio (OSNR) [20, 21].

2.2 Attenuation

Fibre attenuation can be described by the expression given in Eq. (1):

$$^{dP}/_{dz} = -\alpha P \tag{1}$$

where α corresponds to the power attenuation factor per unit length.

If launched power into the fibre cable is P_{in}, then the output power after propagation via the fibre length, L, is given by Eq. (2):

$$P_{out} = P_{in}\, exp^{(-\alpha L)} \tag{2}$$

The absorption coefficient, α, varies with wavelength, λ. This coefficient characterizes the loss measured in decibels per kilometre length of the fibre [22].

Linear characteristic is either initiated by internal or external factors. The internal factor results from impure substances that are inherently present in the fibre during the manufacturing process. When light signals hit any of the impurities, it scatters or is absorbed, leading to an intrinsic loss. This loss can further be classified into two components:

i. The material absorption is caused by imperfection as well as impurities in the fibre.

ii. Rayleigh scattering results from the elastic interactions between the light wave and the glass molecules. It accounts for nearly 96% of attenuation in the optical fibre cable and varies as expressed in Eq. (3):

$$\alpha_R = {}^{c}/_{\lambda^4}, \text{where } C = 0.7 - 0.9\ ({}^{dB}/_{km}) - \mu m^4 \quad (3)$$

On the other hand, extrinsic attenuations are initiated by external stains such as macro or micro bending. Imperfection in the cylindrical geometry of fibre during the manufacturing process leads to a macro bending and can be visible when inspected with the OTDR [6, 23]. In essence, when the bends are corrected, the loss generally is reversible. If loss must be avoided, the minimum bending radius must not exceed ten times the outer diameter of the cable type. Similarly, temperature, tensile stress or severe force may also affect micro-bending [24]. It is irreversible. Both bends will result in the reduction of optical output power.

2.3 OSNR

The IEC standard has defined OSNR as the signal power at the peak of a channel divided by the noise power interpolated at the position of the peak. This definition can be expressed in the form of Eq. (4):

$$OSNR = 10\ log_{10}\left({}^{P_i}/_{N_i}\right) + 10\ log_{10}\left({}^{B_m}/_{B_r}\right) \quad (4)$$

where P_i is the optical signal power at the i^{th}channel,
B_m is the resolution bandwidth,
N_i is the interpolated value of noise power and
B_r is the reference optical bandwidth.
An additional noise can also be added to the entire system by some devices like optical amplifiers, ROADMs and lasers. Thus, in this work, optical amplifier noise has been considered the main source of OSNR limitation and degradation.

2.4 Chromatic dispersion (CD)

Chromatic dispersion in fibre network links is a result of the change in group delay per unit wavelength in ps/nm. It accumulates with distance. The delay coefficient is generally quoted in units of ps/(nm*km) and depends on the fibre type (in this case, G.652).

The graph of group delay versus wavelength was then fitted to data using the approximation equation of (6) in **Table 1**.

2.5 Polarization mode dispersion (PMD)

PMD is measured in pico-seconds (ps) for a span length of installed fibre cables.

The general result of this phenomenon may be a continuous increment in PMD, as given in Eq. (5), the appropriate units that are utilized for the coefficient that characterizes the fibre itself are $ps/km^{1/2}$.

$$PMD_{total} = \left(\sum_n (PMD_n)^2\right)^{1/2} \quad (5)$$

The polarization unit vector, representing the state of polarization (SOP) of the electric field vector, does not remain constant in practical optical fibres; rather, it changes in a random fashion along with the fibre because of its fluctuating

Fit technique	Group delay's equation	Dispersion data's equation	Equation no.
3-term Sellmeier	$A + B\lambda^2 + C\lambda^{-2}$	$2B\lambda + C\lambda^{-3}$	(6)
5-term Sellmeier	$A + B\lambda^2 + C\lambda^{-2} + D\lambda^4 + E\lambda^{-4}$	$2B\lambda^2 - 2C\lambda^{-3} + 4D\lambda^3 - 4E\lambda^{-5}$	(7)
2nd order polynomial (quadratic)	$A + B\lambda + C\lambda^2$	$B + 2C\lambda$	(8)
3rd-order polynomial (cubic)	$A + B\lambda + C\lambda^2 + D\lambda^3$	$B + 2C\lambda + 3C\lambda^2$	(9)
4th order polynomial	$A + B\lambda + C\lambda^2 + D\lambda^3 + E\lambda^4$	$B + 2C\lambda + 3C\lambda^2 + 4E\lambda^3$	(10)
Equations for slope (table A2/ITU-T G650.1)			
Fit technique	Dispersion slope's equation		
3-term Sellmeier	$2B + 6C\lambda^{-4}$		(11)
5-term Sellmeier	$2B + 6C\lambda^{-4} + 12D\lambda^2 + 20E\lambda^{-6}$		(12)
2nd order polynomial (quadratic)	$2C$		(13)
3rd-order polynomial (cubic)	$2C + 6D\lambda$		(14)
4th order polynomial	$2C + 6D\lambda + 12D\lambda^2$		(15)
Equations for zero dispersion wavelength and slope (A.3/ITU G650.1)			
Fit technique	Zero dispersion wavelength	Zero dispersion slope	
3-term Sellmeier	$(C/B)^{1/4}$	$8B$	(16)
2nd order polynomial (quadratic)	$-B/(2C)$	$2C$	(17)

Table 1.
Approximation equations for group delay and dispersion [25].

birefringence. Two common birefringence sources are (1) geometric birefringence (related to small departures from perfect cylindrical symmetry) and (2) anisotropic stress (produced on the fibre core during manufacturing or cabling of the fibre).

The degree of birefringence is described by the difference in refractive indices of orthogonally polarized modes of Eq. (18).

$$B_m = \left|n_x - n_y\right| = \Delta n \tag{18}$$

According to Ref. [26], the corresponding difference in propagation constants of two orthogonally polarized modes is given by Eq. (19).

$$\Delta\beta = \left|\beta_x - \beta_y\right| = (\omega/c)\Delta n \tag{19}$$

Birefringence causes the two polarization components to exchange power periodically, as described by the beat length of Eq. (20).

$$L_B = \frac{2\pi}{\Delta\beta} = \lambda/\Delta n \tag{20}$$

Typically, $B_m. \sim 10^{-7}$, and therefore $L_B \sim$10 m for λ ~1 μm. Linearly polarized light remains linearly polarized only when it is polarized along with one of the

principal axes; otherwise, its polarization state changes along the fibre length from linear to elliptic, then returns to linear, in a periodic manner, over the length L_B

The modal group indices and modal group velocities are related by Eq. (21).

$$n_{gx,y} = \frac{\mathrm{c}}{\mathrm{v_{gx,y}}} = \frac{\mathrm{c}}{\left(1/\beta_{1x,y}\right)} \tag{21}$$

where

$$\beta_{1x,y} = \frac{d\beta_{x,y}}{d\omega} \tag{22}$$

So that the difference in time arrivals (at the end of fibre of length, L) for two orthogonal polarization modes, known as the differential group delay (DGD), can be calculated using Eq. (23).

$$\Delta\tau = \left|\frac{\mathrm{L}}{\mathrm{v_{gx}}} - \frac{\mathrm{L}}{\mathrm{v_{gy}}}\right| = L\left|\beta_{1x} - \beta_{1y}\right| = L\Delta\beta_1 \tag{23}$$

3. Methods

The optical time domain reflectometry technique has been employed in CD measurement. During the process, the OTDR sends pulsations of four or more wavelengths into each of the tested fibre cores so that the comparative arrival time is subsequently measured and recorded for each backscattered wavelength signal [27–29]. The comparison between the reference wavelength and the arrival times of the other wavelengths were computed and fitted to data using the approximation equations of (5) in **Table 1** above.

Similarly, a PMD test set was used to measure PMD. An averaging procedure helps in determining the PMD of several sections of the optical fibre link. The optical spectrum analyzer, OSA, has been deployed to automatically calculate the total PMD of the several spans in the network. This device uses the root mean square summation [30] of Eq. (8).

To characterize the entire network components, the OSA became the protagonist for such tests and measurements at two distinct ports on the WDM system using different wavelengths [31, 32]. The basic measurements in the frequency domain required were:

a. Total power for the optical signal

b. Measurement of channel power

c. OSNR

d. Measurement of central channel wavelength

e. Measurement of the spacing between signals [33]

The measurements were carried out with the FTB 5240S and FTB-5250S-EI instruments, designed with dedicated algorithms for each application.

The characterization measurements of the network [34] components, such as the ROADMs or filters, amplifiers, DFB lasers, FB laser and LED, were determined by the equipment in all scopes of application.

4. Results and discussion

4.1 Experimental process

Two experimental procedures were carried out to ascertain the presence of optical faults on the cable. These were as follows:

4.1.1 Chromatic dispersion (CD)

The obtained CD result is tabulated in **Table 2**. From this experiment, it was observed that the maximum allowable dispersion of 110.682 $ps/nm*km$ appears at 1548.50 *nm* wavelengths. Beyond this wavelength, signals failed to be transmitted due to the presence of CD caused by the 1550 *nm* modulator.

The relationship between the dispersion and the relative group delay (RGD) to wavelength has been presented in **Figure 1** for the 80 km SM fibre cable link. The graph reveals the presence of chromatic dispersion at the targeted wavelength of 1550 nm of the modulator; the value of CD is seen to be 16.696 $ps/(nm*km)$ with a slope of 0.060859 $ps/(nm2*km)$. The RGD-weighted RMS error was 286.313 ps during the 4 seconds average acquisition time over the 0.5 nm wavelength step.

4.1.2 Polarization mode dispersion (PMD)

As depicted in **Figure 2**, the resulting value of PMD for a 40 km fibre length tested was 0.785 ps within the wavelength band of 1514.62–1588.66 nm. The PMD coefficient was 0.1241 $ps/k^{1/2}$ with a Gaussian compliance factor of 1.069.

The PDM and fibre loss over different lengths of optical fibre cable are presented in **Table 3**.

This depicts that both the link polarization dispersion and link losses increased with an increase in cable length.

Table 4 depicts the maximum PMD over a given transmission bit rate. The maximum PMD decreases with an increase in bit rate.

4.2 Drift analysis with WDM investigator

Figure 3 shows how power, wavelengths and OSNR were monitored over time in the SMFOC network. This was achieved using FTBx-5245/5255 OSA with a WDM investigator. The investigation indicates the presence and strength of polarization pulse spreading (PPS) in the tested channels. The controlled emissions of a 50-GHz-spaced 40-DWDM-channel covering the wavelength of 1529.545–1556.54 nm window have been presented. The investigator gave details on the fibre link characteristics. For example, the presence of carved noise from the PoIMux and other types of impairments like carrier leakages, PMD pulse spreading, crosstalk and non-linear effects were also revealed by a certain degree of severity ('OK', 'warning', 'risk') as shown in

Used	Wavelength (nm)	RGD (ps)	Fitted RGD (ps)	RGD deviation (ps)	Pass/ Fail	Dispersion ps/nm	Pass/ fail	Dispersion ps/(nm*km)
Yes	1530.0	0.00	35.472	35.472	Pass	123.519	Pass	103.043
Yes	1530.5	628.78	654.360	25.579	Pass	1239.033	Pass	103.253
Yes	1531.0	1222.47	1274.505	52.039	Pass	1241.544	Pass	103.462
Yes	1531.5	1857.76	1895.904	38.145	Pass	1244.054	Pass	103.671
Yes	1532.0	2488.23	2518.558	30.333	Pass	1246.562	Pass	103.880
Yes	1532.5	3096.88	3142.466	45.583	Pass	1249.067	Pass	104.089
Yes	1533.0	3741.69	3767.626	25.938	Pass	1251.571	Pass	104.298
Yes	1533.5	4388.24	4394.036	5.798	Pass	1254.072	Pass	104.506
Yes	1534.0	4995.16	5021.698	26.537	Pass	1236.572	Pass	104.714
Yes	1534.5	5634.26	5650.608	16.345	Pass	1259.069	Pass	104.922
Yes	1535.0	6275.14	6280.766	5.630	Pass	1261.565	Pass	105.130
Yes	1535.5	6877.73	6912.172	32.447	Pass	1264.058	Pass	105.338
Yes	1536.0	7533.12	7544.824	11.701	Pass	1266.549	Pass	105.546
Yes	1536.5	8187.90	8178.721	9.184	Pass	1269.038	Pass	105.753
Yes	1537.0	8794.54	8813.862	19.319	Pass	1271.526	Pass	105.960
Yes	1537.5	9453.78	9450.246	3.535	Pass	1274.011	Pass	106.168
Yes	1538.0	10093.42	10087.873	5.548	Pass	1274.494	Pass	106.375
Yes	1538.5	10712.04	10726.740	14.698	Pass	1278.975	Pass	106.581
Yes	1539.0	11358.12	11366.848	8.725	Pass	1281.454	Pass	106.788
Yes	1539.5	12006.86	12008.194	1.337	Pass	1283.932	Pass	106.994
Yes	1540.0	12616.22	12650.779	34.556	Pass	1286.407	Pass	107.201
Yes	1540.5	13286.16	13294.601	8.445	Pass	1288.880	Pass	107.407
Yes	1541.0	13947.51	13939.658	7.848	Pass	1291.351	Pass	107.613
Yes	1541.5	14577.69	14585.951	8.262	Pass	1293.820	Pass	107.818
Yes	1542.0	15245.94	15833.478	12.461	Pass	1296.287	Pass	108.024
Yes	1542.5	15901.85	15882.238	19.613	Pass	1298.752	Pass	108.229
Yes	1543.0	16523.19	16532.230	9.040	Pass	1301.216	Pass	108.435
Yes	1543.5	17195.07	17183.454	11.617	Pass	1303.677	Pass	108.640
Yes	1544.0	17856.00	17835.907	20.089	Pass	1306.136	Pass	108.845
Yes	1544.5	18486.43	18489.589	3.155	Pass	1308.593	Pass	109.049
Yes	1545.0	19158.46	19144.500	13.959	Pass	1311.049	Pass	109.254
Yes	1545.5	19822.68	19800.638	22.043	Pass	1313.502	Pass	109.458
Yes	1546.0	20453.18	20458.001	4.822	Pass	1315.953	Pass	109.663
Yes	1546.5	21122.60	21116.590	6.012	Pass	1318.403	Pass	109.867
Yes	1547.0	21787.91	21776.404	11.506	Pass	1320.850	Pass	110.071
Yes	1547.5	22414.29	22437.440	23.147	Fail	1323.295	Pass	110.275
Yes	1548.0	23098.45	23099.699	1.246	Fail	1325.739	Pass	110.478

Used	Wavelength (nm)	RGD (ps)	Fitted RGD (ps)	RGD deviation (ps)	Pass/ Fail	Dispersion ps/nm	Pass/ fail	Dispersion ps/(nm*km)
Yes	1548.5	23785.11	23763.179	21.934	Fail	1328.180	Pass	110.682
Yes	1549.0	22409.30	24427.879	18.578	Fail	1330.620	Fail	110.885
Yes	1549.5	25100.09	25093.798	6.288	Fail	1333.058	Fail	111.088
Yes	1550.0	25770.91	25760.936	9.978	Fail	1335.493	Fail	111.291

Table 2.
Group delay and chromatic dispersion.

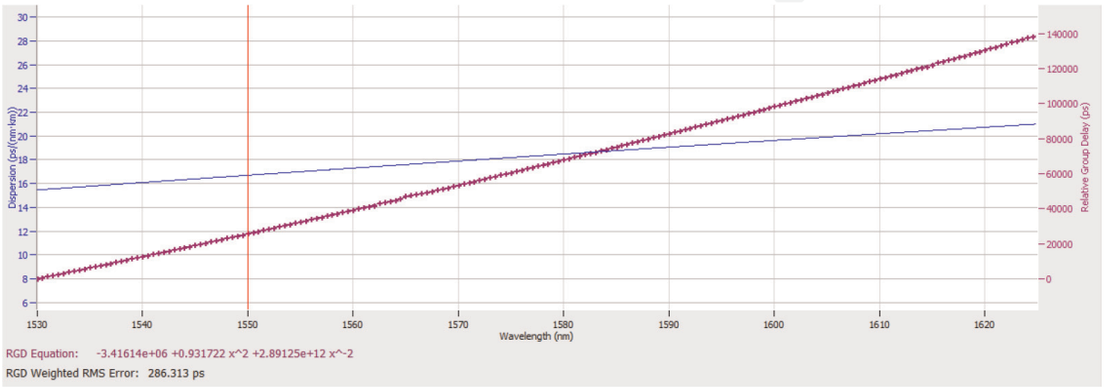

Figure 1.
Chromatic dispersion of 80 km fibre link.

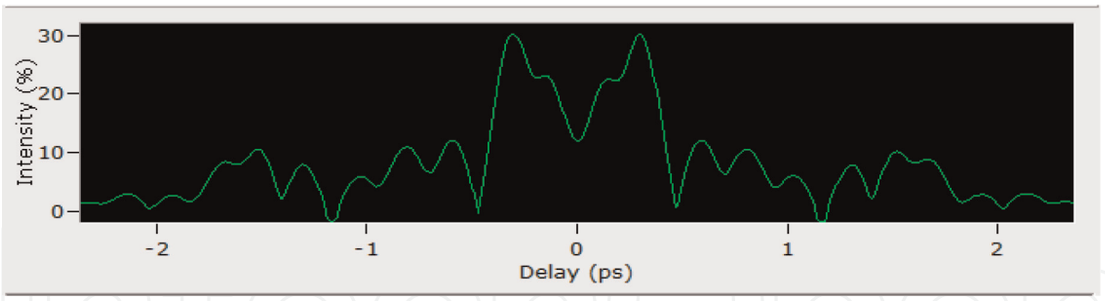

Figure 2.
PMD measured with the interferometry method.

Table 5 below. In this way, the status of the channels tested in a single port was visualized as a trace for any acquisition and change of state.

On the other hand, **Table 6** depicts the channel results for the signal power, OSNR, noise and bandwidth at 3.00 and 20.00 dB, respectively.

It is observed that channel C_025 has the best signal power with a minimum OSNR. Thus, multiple DWDM channels' output power was successfully controlled, and the target level functions were also achieved for the 1550 nm wavelength, as shown in **Figure 4**.

4.3 EDFA analysis

The EDFA was tested and recorded as depicted in **Table 7a** and **b**. OSA traced reports for both the input and output signals of the EDFA under consideration are

Link length (km)	Link PMD (ps)	Link loss (hr/ps)
40	0.785	0.41
200	1.43	0.38
400	2.42	0.18
600	2.53	0.14
800	2.80	0.09
1000	3.09	0.075
1,200	3.54	0.072
1,400	3.68	0.59
1,600	3.99	0.59

Table 3.
Comparison of link PMD and link loss over fibre link length [35].

Bite rate (Gbps)	Maximum PMD (ps)	PMD coefficient ($(ps/km^{1/2})$)
2.5	40	2.0
10	10	0.5
20	5	0.25
40	2.5	0.125

Table 4.
Maximum PMD value for a given bit rate used [35].

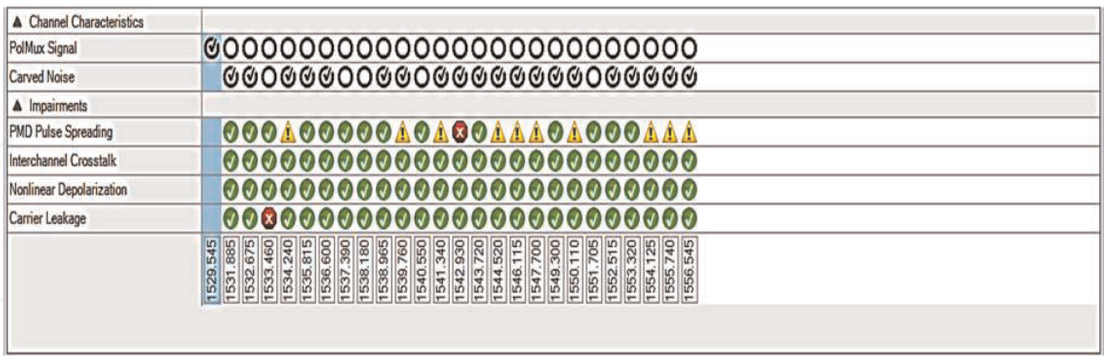

Figure 3.
WDM system with WDM investigator.

depicted in **Figure 5a** and **b**, respectively. From these results, it is observed that better performance of the EDFA has an average wavelength of 1550.42 nm with a total input power of 12.68 *dBm* and power flatness of 3.11 *dB* at the input channel. These parameters' values were, however, depreciated to an average power output of −6.21 *dBm* with a total power of −0.19 *dB* and a power flatness of 2.93 *dB* at the output channel. This is due to additional noise introduced by different active and passive components on the link.

Ch. #	Name	PolMux signal	Carved noise	PMD pulse spreading	Inter-channel crosstalk	Non-linear depolarization	Carrier leakage
1	C_001	Present					
2	C_002	'Not present'	'Present'	'OK'	'OK'	'OK'	'OK'
3	C_003	'Not present'	'Present'	'OK'	'OK'	'OK'	'OK'
4	C_004	'Not present'	Not present	'OK'	OK	OK	'Risk'
5	C_005	'Not present'	'Present'	'Warning'	'OK'	'OK'	'OK'
6	C_006	'Not present'	'Present'	'OK'	'OK'	'OK'	'OK'
7	C_007	'Not present'	'Present'	'OK'	'OK'	'OK'	'OK'
8	C_008	'Not present'	'Not present'	'OK'	'OK'	'OK'	'OK'
9	C_009	'Not present'	'Not present'	'OK'	'OK'	'OK'	'OK'
10	C_010	'Not present'	Present	'OK'	'OK'	'OK'	'OK'
11	C_011	'Not present'	Present	'Warning'	'OK'	'OK'	'OK'
12	C_012	'Not present'	'Not present'	'OK'	'OK'	'OK'	'OK'
13	C_013	'Not present'	Present	'Warning'	'OK'	'OK'	'OK'
14	C_014	'Not present'	'Present'	'Risk'	'OK'	'OK'	'OK'
15	C_015	'Not present'	'Present'	'OK'	'OK'	'OK'	'OK'
16	C_016	'Not present'	'Present'	'Warning'	'OK'	'OK'	'OK'
17	C_017	'Not present'	'Present'	'Warning'	'OK'	'OK'	'OK'
18	C_018	'Not present'	'Present'	'Warning'	'OK'	'OK'	'OK'
19	C_019	'Not present'	'Present'	'OK'	'OK'	'OK'	'OK'
20	C_020	'Not present'	'Present'	'Warning'	'OK'	'OK'	'OK'
21	C_021	'Not present'	'Not present'	'OK'	'OK'	'OK'	'OK'
22	C_022	'Not present'	'Present'	'OK'	'OK'	'OK'	'OK'
23	C_023	'Not present'	'Present'	'OK'	'OK'	'OK'	'OK'
24	C_024	'Not present'	'Present'	'Warning'	'OK'	'OK'	'OK'
25	C_025	'Not present'	'Present'	'Warning'	'OK'	'OK'	'OK'
26	C_026	'Not present'	'Present'	'Warning'	'OK'	'OK'	'OK'

Table 5.
WDM investigator showing information on the fibre link characteristics.

Ch. #	Name	λ (nm)	Signal power (dBm)	OSNR (dB)	Noise (dBm)	BW 3.00 dB (nm)	BW 20.00 dB (nm)
1	C_001	1529.543	(i)-18.17	23.07	(InB)-41.24	0.232	—
2	C_002	1531.883	(i)-19.59	17.63	(InB nf)-37.22	0.138	—
3	C_003	1532.672	(i)-18.06	17.49	(InB nf)-35.55	0.132	0.391
4	C_004	1533.458	(i)-15.83	24.98	(InB)-40.81	0.130	0.299
5	C_005	1534.238	(i)-17.45	17.92	(InB nf)-35.37	0.134	0.384
6	C_006	1535.815	(i)-18.79	18.85	(InB nf)-37.64	0.068	0.313

Ch. #	Name	λ (nm)	Signal power (dBm)	OSNR (dB)	Noise (dBm)	BW 3.00 dB (nm)	BW 20.00 dB (nm)
7	C_007	1536.600	(i)-20.90	16.86	(InB nf)-37.77	0.133	—
8	C_008	1537.391	(i)-16.76	24.69	(InB)-41.45	0.128	0.302
9	C_009	1538.179	(i)-15.82	25.63	(InB)-41.45	0.125	0.276
10	C_010	1538.966	(i)-19.57	18.27	(InB nf)-37.83	0.131	—
11	C_011	1539.757	(i)-19.47	16.62	(InB nf)-36.08	0.139	—
12	C_012	1540.548	(i)-15.65	25.46	(InB)-41.11	0.131	0.296
13	C_013	1541.340	(i)-19.68	16.35	(InB nf)-36.03	0.134	—
14	C_014	1542.927	(i)-18.68	17.67	(InB nf)-36.35	0.136	0.393
15	C_015	1543.720	(i)-18.84	19.18	(InB nf)-38.02	0.135	—
16	C_016	1544.518	(i)-18.64	17.14	(InB nf)-35.79	0.131	0.378
17	C_017	1546.114	(i)-21.48	16.35	(InB nf)-37.83	0.134	—
18	C_018	1547.700	(i)-17.26	20.11	(InB nf)-37.36	0.069	0.285
19	C_019	1549.301	(i)-18.65	17.38	(InB nf)-36.03	0.065	0.323
20	C_020	1550.109	(i)-21.66	15.63	(InB nf)-37.28	0.070	—
21	C_021	1551.704	(i)-15.57	26.07	(InB)-41.64	0.068	0.258
22	C_022	1552.515	(i)-21.38	16.59	(InB nf)-37.97	0.136	—
23	C_023	1553.319	(i)-19.71	18.48	(InB nf)-38.18	0.069	0.333
24	C_024	1554.125	(i)-15.34	21.82	(InB nf)-37.16	0.131	0.285
25	C_025	1555.742	(i)-20.97	16.24	(InB)-37.21	0.068	0.373
26	C_026	1556.543	(i)-19.32	17.52	(InB nf)-36.84	0.068	0.326

Table 6.
Link spectral characterization.

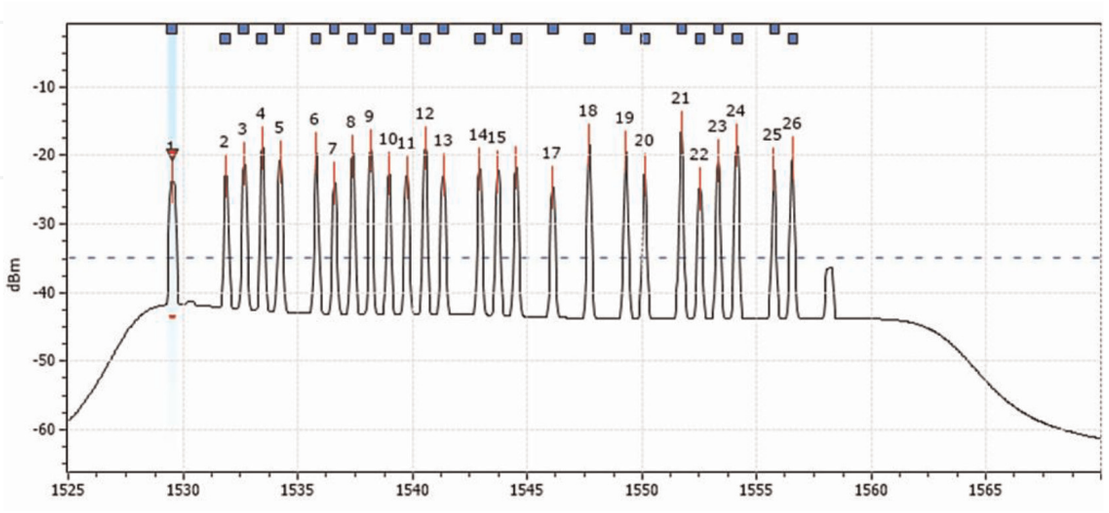

Figure 4.
WDM system characteristic of the link.

(a) Input channel

Peak	Channel	W (nm)	P auto (dBm)	SNR avg. (dB)	Noise avg. (dBm)	Pp (dBm)	Pi (dBm)	Channel Pi (dBm)
1	100G 12	! 1537.347	5.46	45.80	...	5.46	5.26	−2.04
2	100G 24	1546.884	6.84	46.54	...	6.84	7.20	5.63
3	100G 31	1552.512	6.56	44.05	...	6.56	6.56	6.25
4	100G 39	1558.948	8.35	47.60	...	8.35	8.39	6.37
Peak	Channel	BW at 3.00 (nm)	W delta (nm)	Pp–Pavg. (dB)	Pp–Pmax (dB)	<< SNR (dB)	SNR >> (dB)	Worst SNR (dB)
1	100G 12	0.032	...	−1.20	−2.89	45.58	46.04	45.58 <<
2	100G 24	0.036	9.537	0.18	−1.51	46.64	46.45	46.45 >>
3	100G 31	0.044	5.628	−1.42	−2.93	47.09	44.20	43.91 <<
4	100G 39	0.033	6.436	1.69	0.00	50.40	47.75	47.46 <<

Average wavelength	1550.452 nm
Average power	6.66 dBm
Total power	12.48 dBm
Power flatness	3.11 dB

(b) Output channel

Peak	Channel	W (nm)	P auto (dBm)	SNR avg. (dB)	Noise avg. (dBm)	Pp (dBm)	Pi (dBm)	Channel Pi (dBm)
1	100G 12	! 1537.347	−6.18	50.93	...	−6.18	−5.81	−12.36
2	100G 24	1546.884	−6.14	51.14	...	−6.14	−6.49	−7.80
3	100G 31	1552.509	−6.59 i	47.26	...	−7.98	−6.59	−7.00
4	100G 39	1558.948	−5.05	50.48	...	−5.05	−4.98	−7.02
Peak	Channel	BW at 3.00 (nm)	W delta (nm)	Pp–Pavg. (dB)	Pp–Pmax (dB)	<< SNR (dB)	SNR >> (dB)	Worst SNR (dB)
1	100G 12	0.036	...	0.03	−1.13	50.97	50.89	50.89 >>
2	100G 24	0.030	9.537	0.07	−1.09	51.30	50.98	50.98 >>
3	100G 31	0.045	5.625	−1.77	−3.11	43.91	47.47	437.09 <<
4	100G 39	0.034	6.439	1.16	0.00	47.46	50.56	450.56 <<

Average wavelength	1549.367 nm
Average power	−6.21 dBm
Total power	−0.19 dBm
Power flatness	2.93 dB

Table 7.
Optical spectrum analysis of EDFA at 100 GHz over 1500–1600 nm for input and output channel.

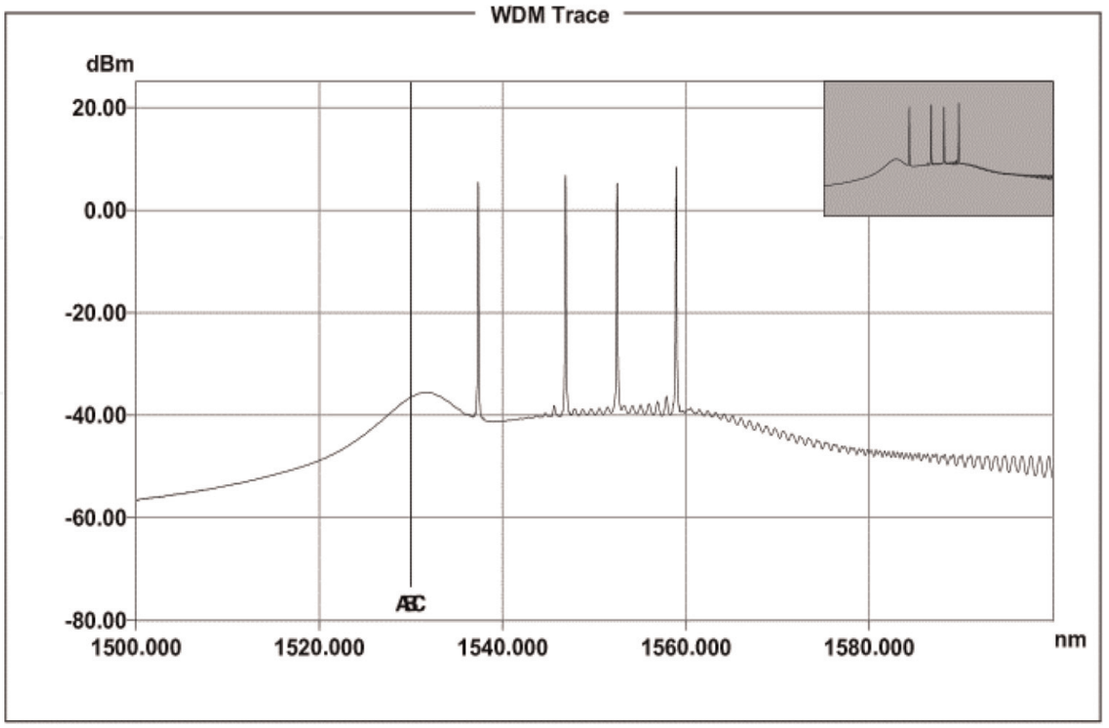

Figure 5.
OSA generated report for the EDFA at 100 GHz and 1500–1600 nm wavelength for input and output channel. (a) Input Channel, (b) Output Channel.

5. Conclusion

In this paper, it was possible to characterize long-distance fibre transmission network systems based on their spectral transmission characteristics. Fibre characterization consists of the measurement and recording of a single span parameter or multiple parameters. The characterization provides documentation for fibre parameters at the time of installation or acquisition for comparison with future measurements to determine fibre degradation due to ageing, damage and repair. This process depends on the transmission system, design margins and the reason for the measurements. At a minimum, the overall fibre loss measurements for operating wavelengths were necessary.

The analysis of the type of single-mode fibre cable for a particular transmission has been seen to be affected by the transmission wavelength. The attenuation and chromatic dispersion were similarly affected by the increase in the distance of communication.

Chromatic dispersion requires more attention in WDM systems using G.652 fibres since the dispersion was seen to be larger in the 1550 nm region. On the other hand, PMD was very noticeable at high bit rates and became alarming at bit rates in excess of 5 Gbps. PMS has been found to be the root cause of impairment in longer-distance optical WDM systems. Hence, to avoid this kind of impairment for transmission systems operating at a bitrate higher than 10 Gbps, PMD fibre compensators with a certain degree of birefringence must be employed to further reduce the impairment to the barest minimum.

An optical spectrum analyzer was used to measure the distribution of optical power energy across the wavelength channel enabling spectral analyses, monitoring of optical signals, assessment of optical amplifier, network analysis and OSNR measurement.

Author details

Asiya E. Asiya[1*], Michael U. Onuu[2], Rufus C. Okoro[3] and O. Enendu Uche[4]

1 Electronics and Computer Technology Unit, University of Calabar, Calabar, Cross River State, Nigeria

2 Engineering Physics Research Group, Department of Physics/Geology/Geophysics, Alex Ekwueme Federal University, Ndufu-Alike, Ebonyi State, Nigeria

3 Faculty of Physical Sciences, Department of Physics, University of Calabar, Calabar, Nigeria

4 Intelligence Information Processing Technology, Department of Computer Engineering, Huzhou University, China

*Address all correspondence to: evangephraim@yahoo.co.uk

References

[1] Govind PA. Fibre-Optic Communication Systems. Rochester, NY: John Wiley; 2021

[2] Zhao T, Wang A, Wang Y, Zhang M, Chang X, Xiong L, et al. Fibre fault location utilizing traffic signal in optical network. Optics Express. 2013;**21**(20): 23978-23984

[3] Song H, Kim BW, Mukherjee B. Long-reach optical access networks: A survey of research challenges, demonstrations, and bandwidth assignment mechanisms. IEEE Communications Surveys & Tutorials. 2010;**12**(1):112-123

[4] Stremler FG. Introduction to Communication Systems. Boston, USA. 1990

[5] Eriksson TA, Bülow H, Leven A. Applying neural networks in optical communication systems: Possible pitfalls. IEEE Photonics Technology Letters. 2017;**29**(23):2091-2094

[6] Kumar V, Rajouria D. Fault detection technique by using OTDR: Limitations and drawbacks on practical approach of measurement. IJETAE. 2012;**2**:283-287

[7] Kyriakopoulos CA, Papadimitriou GI, Nicopolitidis P, Varvarigos E. Energy-efficient lightpath establishment in backbone optical networks based on ant colony optimization. Journal of Lightwave Technology. 2016;**34**(23): 5534-5541

[8] Tanimura T, Hoshida T, Rasmussen JC, Suzuki M, Morikawa H. OSNR monitoring by deep neural networks trained with asynchronously sampled data. In: 2016 21st OptoElectronics and Communications Conference (OECC) Held Jointly with 2016 International Conference on Photonics in Switching (PS). Japan: IEEE; 2016. pp. 1-3

[9] Zhang X, Lu F, Chen S, Zhao X, Zhu M, Sun X. Remote coding scheme based on waveguide Bragg grating in PLC splitter chip for PON monitoring. Optics Express. 2016;**24**(5):4351-4364

[10] Hayford-Acquah T, Asante B. Causes of fiber cut and the recommendation to solve the problem. IOSR Journal of Electronics and Communication Engineering. 2017;**12**(1):46-64

[11] Pournoury M, Moon DS, Nazari T, Kassani SH, Do MH, Lee YS, et al. Low scattering loss fiber with segmented-core and depressed inner cladding structure. Optics Communications. 2014;**317**:13-17

[12] El-Sayed M, Ibrahim PJ, Gunzer F. Investigation of the precision regarding fiber fault location with a commercial optical time domain reflectometer. In: 7th International Symposium on High-Capacity Optical Networks and Enabling Technologies. United States: IEEE; 2010. pp. 237-241

[13] Cohen E, Malka D, Shemer A, Shahmoon A, Zalevsky Z, London M. Neural networks within multi-core optic fibers. Scientific Reports. 2016;**6**(1):1-14

[14] Mo W, Huang YK, Zhang S, Ip E, Kilper DC, Aono Y, et al. ANN-based transfer learning for QoT prediction in real-time mixed line-rate systems. In: 2018 Optical Fiber Communications Conference and Exposition (OFC). California, USA: IEEE; 2018. pp. 1-3

[15] Shiryaev VS, Karaksina EV, Churbanov MF, Kotereva TV, Stepanov BS, Ketkova LA, et al. Special pure germanium-rich Ga-Ge-As-Se glasses

for active mid-IR fiber optics. Materials Research Bulletin. 2018;**107**:430-437

[16] Soujanya A, Goud OSC, Prasad KS, Reddy GP. Featured based pattern analysis using machine learning and artificial intelligence techniques for multiple featured dataset. Materials Today: Proceedings. 2017;**4**(8): 9039-9048

[17] Rubio-Largo A, Vega-Rodriguez MA, GomezPulido JA, Sanchez-Perez JM. A comparative study on multi-objective swarm intelligence for the routing and wavelength assignment problem. IEEE Transactions on Systems, Man and Cybernetics, Part C (Applications and Reviews). 2012;**42**(6):1644-1655

[18] Shahkarami S, Musumeci F, Cugini F, Tornatore M. Machine-learning-based soft-failure detection and identification in optical networks. In: 2018 Optical Fiber Communications Conference and Exposition (OFC). IEEE; 2018. pp. 1-3

[19] Behrens C. Mitigation of Nonlinear Impairments for Advanced Optical Modulation Formats. United Kingdom: UCL (University College London); 2012

[20] Xie C, Möller L. The accuracy assessment of different polarization mode dispersion models. Optical Fiber Technology. 2006;**12**(2):101-109

[21] Jim H. The Reference Guide to Fibre Optics. Santa Monica, CA: The FOA; 2011

[22] Xie F. Optical fibre Line Failure Detecting. Fínland: Vaasa University of Applied Sciences VAMK; 2013

[23] Luo ZQ, Zhang S. Dynamic spectrum management: Complexity and duality. IEEE Journal of Selected Topics in Signal Processing. 2008;**2**(1):57-73

[24] Thongdaeng R, Worasucheep DR. Effect of bending radius and bending location on insertion loss in single mode fibers and polarization maintaining fibers. Procedia Computer Science. 2016; **86**:15-18

[25] Wass J, Thrane J, Piels M, Jones R, Zibar D. Gaussian process regression for WDM system performance prediction. In: 2017 Optical Fiber Communications Conference and Exhibition (OFC). Los Angeles, California, USA: IEEE; 2017. pp. 1-3

[26] Keiser G. Fiber Optic Communications. Massachusetts Ave., NW: Springer Nature; 2021

[27] Urban PJ, Getaneh A, Von der Weid JP, Temporão GP, Vall-llosera G, Chen J. Detection of fiber faults in passive optical networks. Journal of Optical Communications and Networking. 2013;**5**(11):1111-1121

[28] Cen M, Chen J, Mégret P, Moeyaert V, Wuilpart M. Fast and simple fault monitoring for long-reach passive optical networks. In: 2014 The European Conference on Optical Communication (ECOC). Cannes, France: IEEE; 2014. pp. 1-3

[29] Cen M, Chen J, Moeyaert V, Mégret P, Wuilpart M. Multi-wavelength transmission-reflection analysis for fiber monitoring. Optics Express. 2014;**22**(25): 31248-31262

[30] Shtaif M, Mecozzi A, Nagel JA. Mean-square magnitude of all orders of polarization mode dispersion and the relation with the bandwidth of the principal states. IEEE Photonics Technology Letters. 2000; **12**(1):53-55

[31] Park J, Baik J, Lee C. Fault-detection technique in a WDM-PON. Optics Express. 2007;**15**(4):1461-1466

[32] Russell E. Optical Reflections in High-Capacity DWDM Systems, CorningWhite Paper, New York, USA: WP7140. 2020

[33] Collings B, Heismann F, Lietaert G. Reference Guide to Fiber Optic Testing. California, USA: JDS Uniphase Corporation; 2010

[34] https://www.explainthatstuff.com/fiberoptics.html

[35] Makokha J, Odhiambo J. Optical characterization of atmospheric aerosols via airborne spectral imaging and self-organizing map for climate change diagnostics. Open Access Library Journal. 2018;**5**:1-10. DOI: 10.4236/oalib.1104698